High-resolution Fourier-transform emission spectroscopy of the $A\,^4\Pi - X\,^4\Sigma^-$ system of WN

R. S. Ram

Department of Chemistry, University of Arizona, Tucson, Arizona 85721

P. F. Bernath

Department of Chemistry, University of Arizona, Tucson, Arizona 85721, and Department of Chemistry, University of Waterloo, Waterloo, Ontario N2L 3G1, Canada

Received September 1, 1993

The electronic emission spectrum of WN has been observed in the 500–580-nm spectral region with a Fourier-transform spectrometer. The bands were excited in a tungsten hollow-cathode lamp in the presence of a trace of molecular nitrogen. The observed bands have been assigned to the $A\,^4\Pi - X\,^4\Sigma^-$ transition. The ground state is a regular $^4\Sigma^-$ state belonging to Hund's coupling case (a′). The principal ground-state constants obtained from the fit of the observed lines are

$$B_0 = 0.4663779(62), \qquad D_0 = 3.5847(77) \times 10^{-7}, \qquad \gamma_0 = 0.051862(21)\ \mathrm{cm}^{-1}.$$

The excited state, on the other hand, shows Hund's case (c) tendencies with the spin components mixed because of interactions with other neighboring states. There have been no previous observations of the WN molecule to our knowledge.

INTRODUCTION

Solid transition-metal nitrides are well-known hard refractory materials[1] that are formed at high temperatures by the reaction of metals with N_2 or NH_3. In addition to the simple binary nitrides W_2N, WN, and WN_2, tungsten nitrides can also form on tungsten surfaces.[2] The $W{\equiv}N$ triple bond is known in some inorganic complexes.[3]

Although the optical spectra of many gaseous transition-metal oxides and hydrides are relatively well characterized, only a few nitrides are known. Diatomic transition-metal nitrides for which gas-phase data are available include ScN,[4] TiN,[5,6] VN,[7,8] ZrN,[9] NbN,[10,11] and MoN.[12,13] Matrix-isolation studies of some transition-metal nitrides are also available, for example, for TaN,[14] ZrN,[15] MoN,[16,17] and NbN.[18] Gingerich[19] has studied several metal nitrides by mass spectrometry and has predicted a strong bond of 135 kcal/mol for WN on the basis of empirical correlations. However, until the investigation described here, no gas-phase observation of WN has been published to our knowledge. Moreover, there are no *ab initio* calculations available, apart from some corrected effective medium semiempirical calculations aimed at describing tungsten nitride formation on surfaces.[20]

Recently we have initiated a project aimed at increasing the data available for transition-metal oxides, nitrides, and hydrides. We have successfully applied Fourier-transform emission spectroscopy to the detection of near infrared electronic transitions of PtO,[21] NiO,[22] and CoO (Ref. 23) and have reported the first observation of ScN in the gas phase.[4] The $A\,^6\Sigma^+ - X\,^6\Sigma^+$ transition of CrH was reanalyzed,[24] correcting some previous conclusions. In the present paper we report the discovery of another gas-phase transition-metal nitride, WN.

Diatomic transition-metal nitrides are expected to produce complex spectra owing to the high spin coupling of the d electrons, resulting in electronic states with high multiplicity. For example, for MoN the lowest-energy electronic transition has been identified[13] as the $A\,^4\Pi - X\,^4\Sigma^-$ transition. The $X\,^4\Sigma^-$ ground state has a large zero-field splitting of 86 cm^{-1}. Although there are several examples of transitions between quartet states,[25,26] this study of MoN provided the first clear example in which the $^4\Sigma$ state has a large $^4\Sigma_{3/2} - {}^4\Sigma_{1/2}$ spin splitting, thus requiring that the state be classified as Hund's case (a′).[27] Although there is no *ab initio* theoretical work available for WN, the $A\,^4\Pi$ and $X\,^4\Sigma^-$ states of the isovalent MoN have been examined by Allison and Goddard.[28] They predict a $^4\Sigma^-$ ground state with a covalent triple MoN bond. They also predict the first excited state to be of $^4\Pi$ symmetry with the $^4\Pi - {}^4\Sigma^-$ interval of 2.128 eV, which is in good agreement with the experimental results.[13]

WN is expected to have electronic states of the same multiplicity and symmetry as MoN, and the spectra, in general, will lie in the same spectral region. Therefore, by analogy, the bands of WN are expected to involve a $^4\Pi - {}^4\Sigma^-$ transition. The spectra of the different subbands observed for WN are in fact quite similar to those of MoN. Detailed rotational analysis of these bands confirms that indeed a $^4\Pi - {}^4\Sigma^-$ transition is involved, but the excited $^4\Pi$ state of WN shows Hund's case (c) tendencies. For WN each excited-state spin component has to be treated separately, and we retain the Hund's case (a) notation for convenience.

EXPERIMENTS

The WN molecule was made in a tungsten hollow-cathode lamp. The spectra assigned to WN were produced in two different experiments.

0740-3224/94/010225-06$06.00

In the first experiment the plan was to produce a spectrum of the WO molecule. We observed several new bands with moderate intensity when the lamp was operated at 270 V and 250 mA of current with a slow flow of neon at 2.45 Torr of pressure. No O_2 was added, since initially we hoped to clean the cathode before adding oxygen to produce WO. The high-resolution spectrum of these bands showed the presence of characteristic $^{182}W-^{184}W-^{186}W$ isotope splittings, indicating that these bands certainly involved the tungsten atom.

In the beginning it was assumed that the new bands were due to the WO molecule. However, it was surprising to note that these bands quickly disappeared when ~200 mTorr of O_2 was added to the flow of neon. This observation ruled out the possibility of WO as the emitter of these bands, leaving WH and WN as likely candidates. A closer look at the line spacing in the branches ruled out WH. In addition, the bands disappeared when ~70 mTorr of H_2 was added to the discharge. This left the WN as the most likely molecular emitter.

The second experiment was designed to confirm our identification of WN as the carrier of the new bands. In this case 15 mTorr of N_2 was added to the flow of neon, with the other experimental parameters kept the same. This time the newly observed bands appeared with twice the intensity compared with those of the first experiment. This chemical evidence confirmed that WN was the carrier. Most probably there was a trace of N_2 in the system during the first experiment, or, more likely, solid WN impurity was sputtered from the surface.

Once the conditions were established and the emitter was identified, the spectra were recorded with the 1-m Fourier-transform spectrometer associated with the McMath Solar Telescope of the National Solar Observatory. The spectra in the 10 000–30 000-cm^{-1} wave-number region were recorded in two parts. For the 10 000–18 000-cm^{-1} spectral region the spectrometer was operated with a OG570 filter and silicon diode detectors, and a total of nine scans were coadded over 1 h of integration. For the 17 000–30 000-cm^{-1} region the spectrometer was operated with a $CuSO_4$ filter and silicon diode detectors, and five scans were coadded in 30 min of integration. For both regions the spectrometer resolution was set at 0.02 cm^{-1}. The observed WN bands appear with a maximum signal-to-noise ratio of 40:1.

In addition to WN bands there are several bands belonging to N_2 and N_2^+ as well as tungsten and neon atomic lines. The spectra were calibrated by use of the measurements of the neon atomic lines made by Palmer and Engleman.[29] The absolute accuracy of the wave-number scale is expected to be better than ± 0.001 cm^{-1}. However, overlapping lines and unresolved isotopic splittings limited the precision of the observed WN line positions to ± 0.002 cm^{-1}.

GENERAL FEATURES OF THE WN SPECTRUM

The interferograms were transformed by G. Ladd of the National Solar Observatory to give the spectra of WN. The spectral line positions were extracted from the observed spectra with a data-reduction program called PC-DECOMP developed by J. Brault. The peak positions were determined by the fitting of a Voigt line-shape function to each spectral feature with a nonlinear least-squares procedure. The branches in the different subbands were sorted with a color Loomis–Wood program running on a PC computer.

The main bands of WN are present in the 17 000–20 000-cm^{-1} spectral region. The observed spectrum consists of four groups of prominent bands, with the strongest features lying at 17 471.9, 18 375.8, 18 747.5, and 19 830.3 cm^{-1}. These are the 0–0 heads of the four subbands expected for a Hund's case (a) $^4\Pi-^4\Sigma^-$ transition.

After a closer inspection of the rotational structure, the subbands could be classified into two groups. Each of the subbands has six branches, but the 17 472- and the 19 830-cm^{-1} bands have unusual O- and S-form ($-4B$ and $+4B$) branches in addition to the usual P ($-2B$), Q ($\pm 0B$), and R ($+2B$) form branches, whereas the 18 376- and the 18 748-cm^{-1} bands consist of doubled P, Q, and R branches. The rotational analysis of these bands indicates that the 17 472- and the 19 830-cm^{-1} bands involve the $^4\Sigma_{1/2}$ spin component, while the 18 376- and 18 748-cm^{-1} bands have the $^4\Sigma_{3/2}$ spin component as their lower state.

The band at 17 472 cm^{-1} is relatively weak in intensity compared with the other subbands. This is most probably because this band lies close to the wave-number cutoffs of both filters. This band is followed by even weaker band heads at 17 396 and 17 307 cm^{-1} that show larger $^{182}W-^{184}W-^{186}W$ isotope splittings. These bands are, therefore, the 1–1 and 2–2 vibrational bands. Only the 0–0 bands were rotationally analyzed. As is described in detail below, this subband has been assigned as the $^4\Pi_{3/2}-^4\Sigma_{1/2}$ subband.

The 19 830-cm^{-1} band has the same pattern as the 17 472-cm^{-1} band and is the strongest band in our spectrum. This band has been assigned as the $^4\Pi_{1/2}-^4\Sigma_{1/2}$ subband. The 1–1 vibrational band associated with this band lies at 19 723.8 cm^{-1}, ~106 cm^{-1} away from the 0–0 band. It is interesting to note that, even though the 17 472 and 19 830 cm^{-1} bands share a common lower state, the interval of 87 cm^{-1} between the 0–0 and the 1–1 bands in the $^4\Pi_{3/2}-^4\Sigma_{1/2}$ subband is considerably different from that in the $^4\Pi_{1/2}-^4\Sigma_{1/2}$ subband. This means that $^4\Pi_{1/2}$ and $^4\Pi_{3/2}$ spin components of the excited state have quite different vibrational frequencies, which is consistent with their Hund's case (c) tendencies. This is not surprising, since the $^4\Pi_{1/2}$ and $^4\Pi_{3/2}$ spin components are ~2367 cm^{-1} apart (Fig. 1).

The remaining two bands at 18 376 and 18 748 cm^{-1} have been assigned as the $^4\Pi_{-1/2}-^4\Sigma_{3/2}$ and $^4\Pi_{5/2}-^4\Sigma_{3/2}$ subbands. The structure of the $^4\Pi_{-1/2}-^4\Sigma_{3/2}$ subband is more complicated than that of the $^4\Pi_{5/2}-^4\Sigma_{3/2}$ subband because of the large Ω doubling in the $^4\Pi_{-1/2}$ component. The P, Q, and R branches of the $^4\Pi_{-1/2}-^4\Sigma_{3/2}$ subband split into doublets at the lowest observed J, and the splitting increases approximately linearly with increasing J. This band also has two weaker heads on the lower-wave-number side at 18 286.2 and 18 191.5 cm^{-1}. These bands are much weaker that the 0–0 band and show the evidence of isotope splitting consistent with 1–1 and 2–2 vibrational bands.

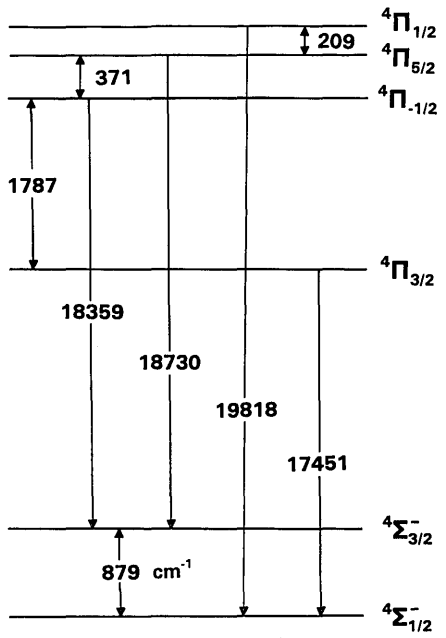

Fig. 1. Energy-level diagram for the $A^4\Pi-X^4\Sigma^-$ electronic transition of WN.

The $^4\Pi_{5/2}-^4\Sigma_{3/2}$ subband at 18 748 cm^{-1} is the simplest band in the spectrum, since the Ω-doubling splitting is not resolved at low J. However, at high J the splitting from the $^4\Sigma_{3/2}$ state becomes apparent, and the lines are also broadened by unresolved isotope structure. The rotational analysis of this band was straightforward, since the first line in the R branch was clearly visible. The $^4\Pi_{5/2}-^4\Sigma_{3/2}$ subband provided the key for the rotational analysis of the other subbands. On the lower-wave-number side of this band there are heads at 18 651.3 and 18 540.3 cm^{-1}, assigned to the 1–1 and 2–2 bands.

The detailed rotational analysis of only the 0–0 bands of each subband was performed. The transition wave numbers of the assigned lines in different subbands are available from the authors.

In addition to the bands discussed so far, there are several isolated bands in the region from 15 000 to 24 000 cm^{-1}. The most prominent heads are at 15 492.3, 20 574.6, 20 725.9, 20 782.8, 21 244.8, 22 347.1, 23 145.7, 23 178.4, and 23 268.9 cm^{-1}. These bands are much weaker in intensity than the bands assigned to the $A^4\Pi-X^4\Sigma^-$ transition. Some of these bands could be associated with the $A^4\Pi$ state or the $X^4\Sigma^-$ state or with entirely new states. Even the possibility of transitions involving doublet states may not be ruled out, since Merer *et al.*[26] recently found many doublet states of VO. The VO molecule is isovalent with WN and has an analogous $A^4\Pi-X^4\Sigma^-$ transition at 10 500 cm^{-1}.

RESULTS AND DISCUSSION

The energy levels of $^4\Pi$ and $^4\Sigma$ states have been treated in great detail by several workers.[13,30–33] We attempted to fit the observed wave numbers of the WN bands with the usual N^2 Hamiltonian defined by Brown *et al.*[34] An explicit listing of the $^4\Pi$ and $^4\Sigma$ matrix elements using Hund's case (a) basis functions is provided by Cheung *et al.*[25] This fit was unsuccessful.

Dunn and co-workers[13] found that the various spin components of the $^4\Pi$ state MoN are affected by interactions with nearby states. They therefore treated the term energy of each substrate separately by replacing ^eT_v with T_Ω ($\Omega = -1/2, 1/2, 3/2, 5/2$). In WN we find that these interactions with nearby states are more severe. As can be seen in Fig. 1, the different spin components are irregularly shifted relative to each other, and there is no obvious order. Therefore we treated each spin component of the excited state separately. Since the ground state belongs to case (a′), in the beginning we treated both spin components $^4\Sigma_{1/2}$ and $^4\Sigma_{3/2}$ separately and later combined them to obtain a single set of $^4\Sigma^-$ constants. Since the subbands having $^4\Sigma_{1/2}$ and $^4\Sigma_{3/2}$ lower states have quite different rotational patterns, we discuss the analysis of the two groups of bands separately.

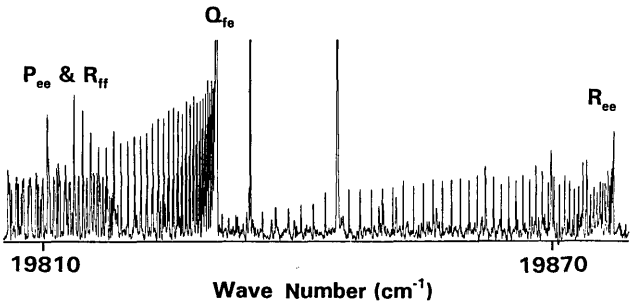

Fig. 2. Portion of the 1/2–1/2 subband of the $A^4\Pi-X^4\Sigma^-$ system of WN.

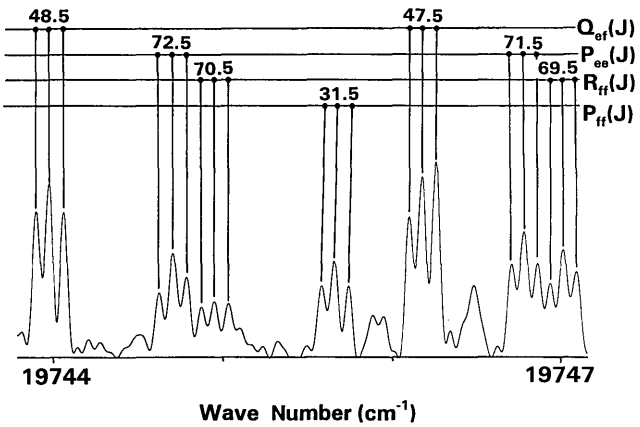

Fig. 3. Portion of the 1/2–1/2 subband of WN at high J, showing the isotope splittings that are due to the ^{182}WN–^{184}WN–^{186}WN isotopomers.

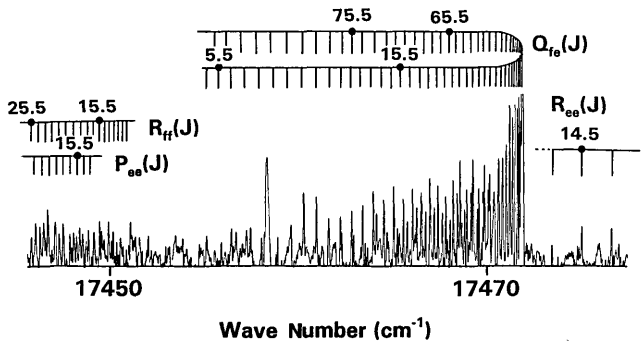

Fig. 4. Portion of the 3/2–1/2 subband of the $A^4\Pi-X^4\Sigma^-$ system of WN.

Table 1. Spectroscopic Constants (cm^{-1}) for the $A\,^4\Pi_\Omega$ Substates of WN[a]

Constants	$^4\Pi_{-1/2}$	$^4\Pi_{1/2}$	$^4\Pi_{3/2}$	$^4\Pi_{5/2}$
T_v	18359.4584(6)	19818.2372(6)	17451.2251(8)	18730.1016(5)
B_v	0.453900(11)	0.4518003(81)	0.4566123(81)	0.454875(11)
$10^{-7} \times D_v$	3.848(22)	4.0024(80)	3.9018(84)	3.973(22)
p_v	−0.01127(48)	0.10616(35)	—	—
$10^{-7} \times p_{Dv}$	2.16(24)	−4.205(81)	−0.95(14)	—

[a]Each spin component in both the ground and the excited state was treated as a separate state.

Table 2. Spectroscopic Constants (cm^{-1}) for the $X\,^4\Sigma_\Omega$ Spin Components of WN[a]

Constants	$^4\Pi_{1/2}$	$^4\Sigma_{3/2}$
B_v	0.4658183(81)	0.466928(11)
$10^{-7} \times D_v$	3.5779(83)	3.568(23)
p_v	1.762124(31)	0.000204(28)
$10^{-6} \times p_{Dv}$	4.0740(84)	−1.3577(93)

[a]Each component was fitted separately.

Bands with a $^4\Sigma_{1/2}$ Lower State

As was discussed in detail by Kopp and Hougen[27] and by Carlson *et al.*,[13] the $^4\Sigma_{1/2}$ state has a large effective Ω doubling, with the Ω-doubling constant p given by

$$p \approx +(-1)^{S+1/2}(2S + 1)B_{1/2} = 4B \qquad (1)$$

for $S = 3/2$. This results in branches with $\pm B$, $\pm 2B$, and $\pm 4B$ spacings for a $^4\Pi - ^4\Sigma_{1/2}$ transition if $B' \approx B''$. The $\Delta\Sigma = 0$ selection rule appropriate for Hund's case (a) limits the observed transitions to $^4\Pi_{3/2} - ^4\Sigma_{1/2}$ and $^4\Pi_{1/2} - ^4\Sigma_{1/2}$.

Part of the spectrum of the 1/2–1/2 subband is displayed in Fig. 2 with the head-forming branches marked. The R_{ee} branch is an S-type branch and forms a head at 19877.3 cm^{-1}. The Q_{fe} branch is the $+2B$ branch and forms a head at 19830.3 cm^{-1}. The two $\pm 0B$ (Q-form) branches run toward the lower-wave-number side with increasing J. The remaining two branches ($-2B$ and $-4B$) are not shown in this figure.

Tungsten has five naturally occurring isotopes ^{180}W (0.1%), ^{182}W (26.3%), ^{183}W (14.3%), ^{184}W (30.7%), and ^{186}W (28.6%). At higher J the splitting resulting from these isotopic species is resolved. To illustrate this, part of the spectrum of WN at high J is given in Fig. 3. The characteristic triplet pattern is due to the more abundant ^{182}WN, ^{184}WN, and ^{186}WN isotopomers, with the central peak due to the most abundant ^{184}WN isotopomer. The linewidth of each isotopic line at high J is approximately 0.045 cm^{-1}. In the region where the isotopic lines are not resolved, the lines are much broader and, therefore, were weighted accordingly in the final fit.

The $^4\Pi_{3/2} - ^4\Sigma_{1/2}$ subband at 17472 cm^{-1} has a pattern similar to the 1/2–1/2 subband. A part of the rotational structure of this subband is shown in Fig. 4.

Initially the lines of the $^4\Pi_{1/2} - ^4\Sigma_{1/2}$ and $^4\Pi_{3/2} - ^4\Sigma_{1/2}$ subbands were fitted separately, and the lower-state constants obtained from these fits were in excellent agreement with each other. Next both of these subbands were fitted together for the determination of a single set of effective rotational constants for the $X\,^4\Sigma_{1/2}$ state. In this fit both the excited states were fitted independently as Hund's case (c) states by use of the expression[13]

$$F(J) = T_v + BJ(J + 1) - D[J(J + 1)]^2 \pm 1/2[p(J + 1/2) + p_D(J + 1/2)^3]. \qquad (2)$$

For the lower $^4\Sigma_{1/2}$ state the corresponding Hund's case (a′) expression is[13,27]

$$F(J) = T_v + BJ(J + 1) - D[J(J + 1)]^2 \pm 1/2[-p(J + 1/2) + p_D(J + 1/2)^3]. \qquad (3)$$

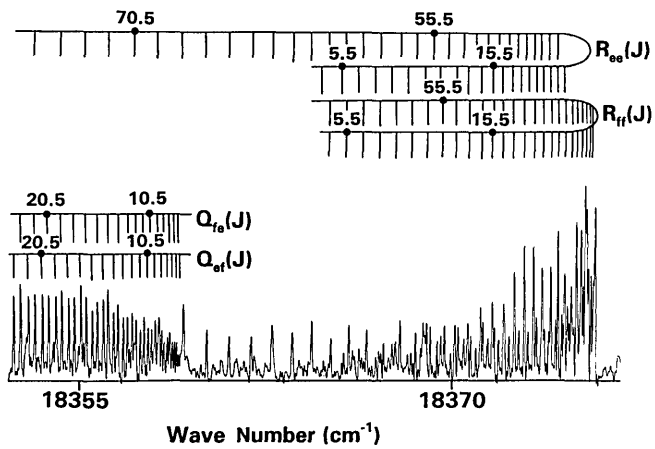

Fig. 5. Portion of the $-1/2-3/2$ subband of the $A\,^4\Pi - X\,^4\Sigma^-$ system of WN.

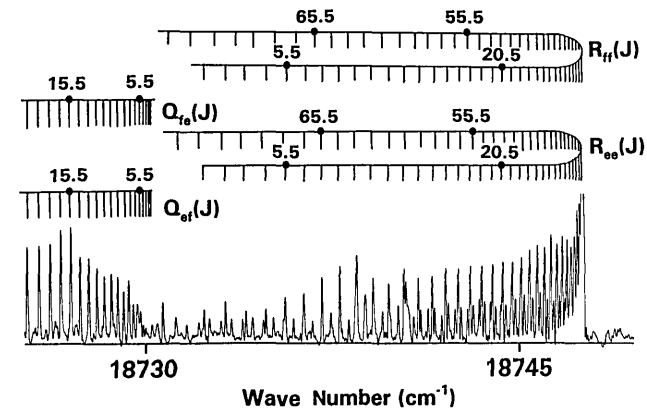

Fig. 6. Portion of the 5/2–3/2 subband of the $A\,^4\Pi - X\,^4\Sigma^-$ system of WN.

Table 3. Spectroscopic Constants (cm^{-1}) for the $A\,^4\Pi_\Omega$ Substates of WN[a]

Constants	$^4\Pi_{-1/2}$	$^4\Pi_{1/2}$	$^4\Pi_{3/2}$	$^4\Pi_{5/2}$
T_v	18798.3306(6)	19380.2719(6)	17013.2597(8)	19168.9739(6)
B_v	0.4539113(76)	0.4517927(75)	0.4566049(76)	0.4548863(76)
$10^{-7} \times D_v$	3.8810(79)	3.9925(76)	3.8926(77)	4.0056(75)
p_v	−0.01128(53)	0.106187(34)	—	—
$10^{-7} \times p_{Dv}$	2.29(27)	−4.285(77)	−0.98(14)	—

[a]Each excited-state spin component was treated as a separate state, but the two lower-state spin components were fitted together.

In Eq. (3) the negative sign in front of p is retained for consistency with the paper by Kopp and Hougen.[27] The constants obtained for the excited states are provided in Table 1, and the lower-state constants obtained for the $^4\Sigma_{1/2}$ state are provided in Table 2.

Relation (1) for p, obtained by Kopp and Hougen[27] for Hund's case (a′) $^4\Sigma_{1/2}$ state, can be tested. The value of $4B$ is 1.86 cm^{-1}, which compares well with the observed value of 1.76 cm^{-1}. The deviations from relation (1) are presumably due to interactions with other electronic states.

Bands with a $^4\Sigma_{3/2}$ Lower State

The 18376- and 18747-cm^{-1} bands have the $^4\Sigma_{3/2}$ spin component as their lower state. These bands have been assigned as $^4\Pi_{-1/2}-{}^4\Sigma_{3/2}$ and $^4\Pi_{5/2}-{}^4\Sigma_{3/2}$ transitions on the basis of Ω doubling in the excited states, since the $^4\Pi_{-1/2}$ component should have a large Ω doubling compared with the $^4\Pi_{5/2}$ state. The structure of these bands consists of $\pm 0B$ and $\pm 2B$ branches. Also, a small Ω doubling has been determined in the lower $^4\Sigma_{3/2}$ state.

A part of the spectrum of the $^4\Pi_{-1/2}-{}^4\Sigma_{3/2}$ subband is displayed in Fig. 5. The spectrum consists of P, Q, and R branches, each doubled owing to large Ω doubling in the excited $^4\Pi_{-1/2}$ state. A part of the spectrum of the $^4\Pi_{5/2}-{}^4\Sigma_{3/2}$ subband is provided in Fig. 6.

In the beginning these two bands were fitted separately and were later combined for the determination of a single set of constants for the lower $^4\Sigma_{3/2}$ state. Also in this case the excited $^4\Pi_{-1/2}$ and $^4\Pi_{5/2}$ substates were treated as separate states. The rotational constants obtained for the $^4\Pi_{-1/2}$ and $^4\Pi_{5/2}$ substates are provided in Table 1, and the constants for the $^4\Sigma_{3/2}$ spin component are provided in Table 2. For the $^4\Sigma_{3/2}$ state, Eq. (2) was used to represent the rotational energy levels.

Constants for the $X\,^4\Sigma^-$

In the initial fits the $^4\Sigma_{1/2}$ and $^4\Sigma_{3/2}$ spin components were treated separately. In the final fit we tried to determine a single set of constants for the $X\,^4\Sigma^-$ state by combining the data for all the subbands. The excited states of all the subbands were still treated as four separate states.

The interval between the $^4\Sigma_{3/2}$ and the $^4\Sigma_{1/2}$ spin components is given by 4λ. The λ parameter is called the spin–spin constant, but the major contribution is from second-order spin–orbit coupling. Since tungsten is a heavy element with an open $5d$ shell, the spin–orbit coupling constant will be large, and $\lambda \gg B$. Not surprisingly then, λ was not well determined in the combined fit, since we have no direct connection between the two spin components. The value of λ was allowed to vary in a preliminary fit to give a value of $\lambda = 219.65 \pm 0.45$ cm^{-1}. The estimated uncertainty in λ has no meaning, because the error is dominated by systematic errors from interactions with other nearby electronic states. In fact this value of λ could easily be in error by 10–100 cm^{-1}.

For the final fit the value of λ was fixed at 219.65 cm^{-1}. The excited-state constants obtained from this fit are provided in Table 3, and the ground state $X\,^4\Sigma^-$ constants obtained in the final fit are provided in Table 4.

The extremely large value of λ obtained from this fit indicates that the ground state has a very large zero-field splitting of ~879 cm^{-1}. The standard deviation of the combined final fit was the same as the two separate fits, indicating that the $^4\Sigma^-$ state is a relatively isolated Hund's case (a′) state.

There is a perturbation in the f parity of the $A\,^4\Pi_{3/2}$ spin component at $J = 60.5$. We do not have sufficient data to identify the perturbing state, so that the perturbed lines were excluded from the final fit.

The $A\,^4\Pi$ state of WN is an interesting example of a state that displays clear Hund's case (c) tendencies, yet the $^{2S+1}\Lambda$ parentage can still be ascertained. The main clues for this purpose are the Ω doubling and comparison with the isovalent MoN molecule. First lines were generally not found, so that reliable Ω values could not be determined from them. However, the Ω doubling splitting should increase as $J^{2\Omega}$ as J increases. As expected, the $^4\Pi_{5/2}$ state shows no doubling, the small splitting in the $^4\Pi_{3/2}$ state increases as J^3, while the $^4\Pi_{1/2}$ and the $^4\Pi_{-1/2}$ states have large linear Ω doubling (Table 3).

As was predicted by Budò and Kovacs,[30] the Ω-doubling constant p should be large and negative for the $^4\Pi_{-1/2}$ substate and of approximately the same magnitude but positive for the $^4\Pi_{1/2}$ substate. Although the signs are correct (Table 3), the magnitude of p differs by a factor

Table 4. Spectroscopic Constants (cm^{-1}) for the $X\,^4\Sigma^-$ State of WN[a]

Constants	$X\,^4\Sigma^-$
B_v	0.4663779(62)
$10^{-7} \times D_v$	3.5847(77)
$10^{-2} \times \gamma_v$	5.1862(21)
$10^{-8} \times \gamma_{D_v}$	−3.76(47)
λ_v	219.65[b]
$10^{-5} \times \lambda_{Dv}$	−2.51(11)

[a]Both spin components were fitted together, but the excited-state spin components were fitted as separate states.
[b]Fixed; see text for details.

Table 5. r_0 (Å) Values for the Ground and the Excited States of WN

State	r_0 (Å)
$X\,^4\Sigma^-$	1.66667(1)
$A\,^4\Pi_{-1/2}$	1.68940(1)
$A\,^4\Pi_{1/2}$	1.69336(1)
$A\,^4\Pi_{3/2}$	1.68441(1)
$A\,^4\Pi_{5/2}$	1.68759(1)

of 10 for these two states. We take this as an additional indication of Hund's case (c) behavior. The interactions with other electronic states are less severe in MoN, so that $p = -0.173$ cm^{-1} for the $^4\Pi_{-1/2}$ spin component and $p = 0.225$ cm^{-1} for the $^4\Pi_{1/2}$ spin component.[13]

The rotational constants obtained from the combined fit have been used to evaluate r_0 bond lengths for WN in its ground and excited states. The values obtained are provided in Table 5. Interestingly, the r_0 value for the ground state (1.66667 Å) agrees almost exactly with the $W{\equiv}N$ bond length of 1.68 Å determined by x-ray crystallography of an inorganic complex.[3] However, the values obtained by Raeker and DePristo[20] in their semiempirical calculations are considerably different from the experimental value.

CONCLUSION

We have observed the $A\,^4\Pi - X\,^4\Sigma$ transition of the previously unknown WN molecule. The excited-state spin components are shifted relative to one another because of strong interactions with unknown nearby electronic states, and the excited $A\,^4\Pi$ state has Hund's case (c) tendencies. The ground $X\,^4\Sigma^-$ state has a very large zero-field splitting of ~879 cm^{-1} between the $^4\Sigma_{3/2}$ and the $^4\Sigma_{1/2}$ spin components. However, since the two ground-state spin components could be fitted together with a $^4\Sigma^-$ Hamiltonian, the $X\,^4\Sigma^-$ state obeys Hund's case (a′) coupling. The $W{\equiv}N$ triple bond length of 1.66667(1) Å determined for the ground state is in excellent agreement with a bond length of an inorganic complex determined by x-ray crystallography.

ACKNOWLEDGMENTS

We thank J. Wagner, C. Plymate, and P. Hartmann of the National Solar Observatory for assistance in obtaining the spectra. The National Solar Observatory is operated by the Association of Universities for Research in Astronomy, Inc., under contract with the National Science Foundation. The research described here was supported by funding from the Petroleum Research Fund administered by the American Chemical Society. Support was also provided by the Center of Excellence in Molecular and Interfacial Dynamics.

REFERENCES

1. C. L. Rollinson, in *Comprehensive Inorganic Chemistry* (Pergamon, Oxford, 1973), Vol. 3, p. 751.
2. C. T. Rettner, H. Stein, and E. K. Schweizer, J. Chem. Phys. **89,** 3337–3341 (1988).
3. R. A. Wheeler, R. Hoffmann, and J. Strähle, J. Am. Chem. Soc. **108,** 5381–5387 (1986).
4. R. S. Ram and P. F. Bernath, J. Chem. Phys. **96,** 6344–6347 (1992).
5. T. M. Dunn, L. K. Hanson, and K. A. Rubinson, Can. J. Phys. **48,** 1657–1663 (1970).
6. J. K. Bates, N. L. Ranieri, and T. M. Dunn, Can. J. Phys. **54,** 915–916 (1976).
7. S. L. Peter and T. M. Dunn, J. Chem. Phys. **90,** 5333–5336 (1989).
8. B. Simard, C. Masoni, and P. A. Hackett, J. Mol. Spectrosc. **136,** 44–55 (1989).
9. J. K. Bates and T. M. Dunn, Can. J. Phys. **54,** 1216–1223 (1976).
10. T. M. Dunn and M. K. Rao, Nature (London) **222,** 266–267 (1969).
11. J.-L. Fémènias, C. Athénour, and T. M. Dunn, J. Chem. Phys. **63,** 2861–2867 (1975).
12. J. C. Howard and J. G. Conway, J. Chem. Phys. **43,** 3055–3057 (1965).
13. R. C. Carlson, J. K. Bates, and T. M. Dunn, J. Mol. Spectrosc. **110,** 215–241 (1985).
14. J. K. Bates and D. M. Gruen, J. Chem. Phys. **70,** 4428–4429 (1979).
15. J. K. Bates and D. M. Gruen, High Temp. Sci. **10,** 27–43 (1978).
16. J. K. Bates and D. M. Gruen, J. Mol. Spectrosc. **78,** 284–287 (1979).
17. L. B. Knight and J. Steadman, J. Chem. Phys. **76,** 3378–3384 (1982).
18. D. W. Green, W. Korfmacher, and D. M. Gruen, J. Chem. Phys. **58,** 404–405 (1973).
19. K. A. Gingerich, J. Chem. Phys. **49,** 19–24 (1968).
20. T. J. Raeker and A. E. DePristo, Surf. Sci. **235,** 84–106 (1990).
21. C. I. Frum, R. Engleman, Jr., and P. F. Bernath, J. Mol. Spectrosc. **150,** 566–575 (1991).
22. R. S. Ram and P. F. Bernath, J. Mol. Spectrosc. **155,** 315–325 (1992).
23. R. S. Ram, C. N. Jarman, and P. F. Bernath, J. Mol. Spectrosc. **160,** 574–584 (1993).
24. R. S. Ram, C. N. Jarman, and P. F. Bernath, J. Mol. Spectrosc. **161,** 445–454 (1993).
25. A. S.-C. Cheung, A. W. Taylor, and A. J. Merer, J. Mol. Spectrosc. **92,** 391–409 (1982).
26. A. J. Merer, G. Guang, A. S.-C. Cheung, and A. W. Taylor, J. Mol. Spectrosc. **125,** 465–503 (1987).
27. I. Kopp and J. T. Hougen, Can. J. Phys. **45,** 2581–2596 (1967).
28. J. N. Allison and W. A. Goddard, Chem. Phys. **81,** 263–271 (1983).
29. B. A. Palmer and R. Engleman, *Atlas of the Thorium Spectrum* (Los Alamos National Laboratory, Los Alamos, N. Mex., 1983).
30. A. Budò and I. Kovacs, Phys. Z. **45,** 122–126 (1944).
31. L. Veseth, Phys. Scr. **12,** 125–128 (1975).
32. J.-L. Fémènias, Can. J. Phys. **55,** 1733–1774 (1977).
33. J. M. Brown and A. J. Merer, J. Mol. Spectrosc. **74,** 488–494 (1979).
34. J. M. Brown, E. A. Colbourn, J. K. G. Watson, and F. D. Wayne, J. Mol. Spectrosc. **74,** 425–436 (1979).